Laakso, A.; Romanoff, J.; Remes, H.

Free flexural vibration of symmetric beams with inertia induced cross section deformations

Published in:
Thin-Walled Structures

DOI:
10.1016/j.tws.2017.05.032

Published: 30/05/2017

Document Version
Peer-reviewed accepted author manuscript, also known as Final accepted manuscript or Post-print

Free flexural vibration of symmetric beams with inertia induced cross section deformations

A. Laakso[1], J. Romanoff, H. Remes

Department of Mechanical Engineering, Aalto University School of Engineering, P.O. Box 15300, 00076 Aalto, Finland

Abstract

Beams with large thin-walled cross sections are not generally following the classical beam theories such as Euler-Bernoulli and Timoshenko theories. In free vibration, the cross section is deformed by the inertia induced body loads. These deformations may have significant effect on the beam modal frequencies, especially in applications involving non-structural masses. This paper presents a method to include the effect into vibration modal results obtained by the classical beam theories. Generalized mass and stiffness of the classical results are modified according to kinetic-, and strain energies of the cross section deformation. The method is validated in typical engineering case studies against fine mesh Finite Element Method and excellent agreement is found.

Keywords: Modal analysis, Beam theory, Generalized mass, Generalized stiffness, Thin-walled, Finite Element Method

Latin Symbols

A	Amplitude, (Area in Eq. (47))
b	Breadth
$\mathbf{e}$	Unit vector
E	Young's modulus
f	Frequency in Hz
G	Shear modulus
h	Height
I	Second moment of area
K	Generalized Stiffness
L	Length
m	Mass per unit length of beam
M	Generalized Mass

[1]Corresponding author. Tel: +358408489861. E-mail: aleksi.laakso@aalto.fi

q	Distributed load
r	Response
S	Stiffener spacing
t	Time
T	Kinetic energy
U	Strain energy
w	Displacement
x, y, z, s, n	Coordinates

Greek Symbols

δ	Convergence limit
θ	Thickness
λ	Wave length
ν	Poisson's ratio
ξ	Generalized coordinate
ρ	Mass density of the material
Ψ	Deflection mode shape
ω	Frequency in rads^{-1}

Subscripts & Superscripts

*	Corrected value
B	Global beam
C	Cross section
CR	Cross section quantity Relative to global point unit amplitude enforced harmonic motion
dyn	Dynamic
ef	Effective
i	Mode number
n	Iteration step number
$peak$	Peak value
PU	Periodic unit
S	Stiffener
sta	Static

1 Introduction

Beams with thin-walled cross sections are used in several fields of structural engineering including applications in marine, aerospace and bridge structures due to their excellent stiffness to weight ratio. Several models have been developed for modal analysis of these thin-walled beams. Euler-Bernoulli beam model [1] is accurate for slender beams with small cross section dimensions relative to length of flexural waves of the studied vibration mode. Due to its simplicity and availability on commercial Finite Element software, the model is still widely used in practical engineering. The shear-deformations can be accounted by Timoshenko beam theory [2, 3, 4] that provides significantly more accurate modal frequencies in beams that are deep relative to the length of flexural waves of the studied vibration mode. Drawback of practical applicability of Timoshenko's beam model has been definition of shear correction factors for different cross sections; see for example Refs. [5,6,7,8]. However, these methods cannot account the influences of local deformations that occur solely on the beam cross-section plane.

Effects of inertia induced cross section deformations have been studied by NACA in the 1950s & 60s. The phenomenon was observed in vibration tests of box beams [9] and the effect has been analyzed for box beams in [10]; monocoques in [11]; angled sections in [12] and channel sections in [13]. Several bridge beams were studied in [14] by including cross section deformation into equations of motion. Generalized beam theory has been developed to take all the above-mentioned effects elegantly into account inside the beam formulation [15]. It has been applied for vibration problems for example in [16]. Carrera et al. have applied unified formulation [17] to Finite element vibration analysis of arbitrary beams [18]. The unified formulation allows any order beam theory to be systematically analyzed by one-dimensional Finite Element Method. Complicated structures have been studied by the method in [19, 20]. Beams with non-structural masses have been studied in [21, 22]. High order generalized beam theories give accurate result in comparison with 3D FE-models. However, even if these analyses require significantly less computational effort than the 3D FEM, several hundred DOFs are still needed. Thus, there is a need to develop the classical simple beam models further to account the effects of local cross-section deformations on the global beam level modes.

This paper provides a method to take the inertia induced local deformation effects into account in classical beam theories. The correction is based on the energy involved in the cross section deformation. It can be used to correct the beam modal results independent of the solution of the beam problem. This allows use of detailed numerical models where necessary, while carrying out straightforward parts of the problem effectively by simple analytical formulae. This kind of approach has value in conceptual design of structures in which the accuracy of solutions must be reasonable, while the computational cost must be extremely light.

2 Method definition

2.1 Assumptions & Limitations

The beam axis is denoted with x-coordinate, while the vertical direction is denoted by z-coordinate. This study is limited to analysis of beams with symmetric cross sections with respect to xz-plane. Applied coordinate system, and structural dimensions are presented in Figure 1a. Cross section coordinate s goes around centerline of the cross section, and n is perpendicular to s.

Small amplitude free vibration is assumed. Cross sections are assumed to have global reference points(s) that follow global bending behavior of the beam axis. The global reference points are defined in stiff points of the cross section, typically in intersections of plated parts. This study includes thin-walled cross sections, in which thicknesses θ are significantly smaller than cross section main dimensions ($\theta \ll b$ & $\theta \ll h$). Examples of possible cross sections and their global reference points are presented in Figure 1b.

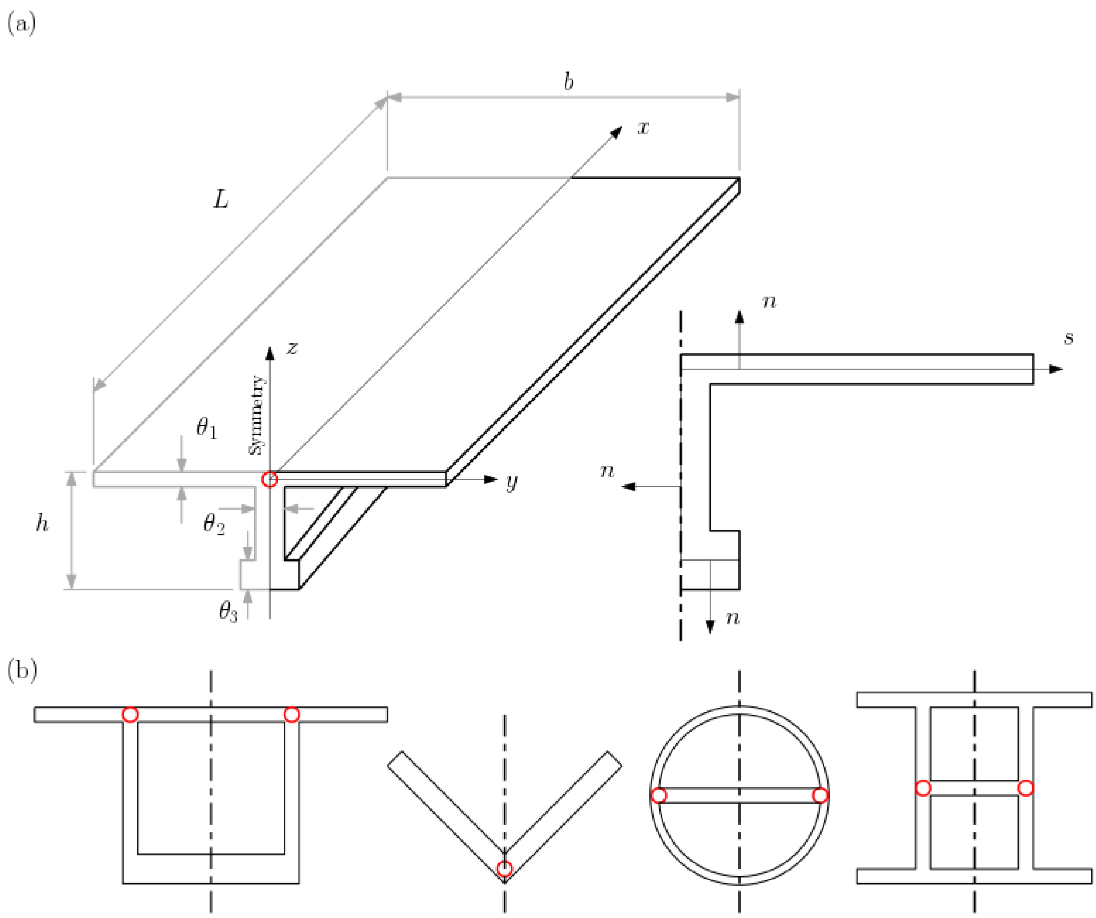

Figure 1. (a) Definition of coordinate systems and dimensions. (b) Examples of thin-walled symmetric cross sections, global reference points indicated by circles.

Length of flexural waves of beam vibration is assumed long in comparison with cross section dimensions ($b \ll \lambda$ & $h \ll \lambda$). This means that locally in a point of cross section, the transversal bending stiffness of cross section dominates the longitudinal bending stiffness by nodes of the global wave. This is also known as cylindrical bending assumption in the cross section analysis.

Additionally, Euler Bernoulli beam is applied in theory definition of Chapter 2. This means that Kinetic energy is assumed purely translational and all strain energy is caused by bending deformation.

2.2 Mode shape definition

Free vibration of a beam at mode i is considered. The beam is vibrating in xz-plane harmonically at the modal angular frequency ω_i. The displacement, $\mathbf{w}_i$, can be written as:

$$\mathbf{w}_i(x, s, \omega_i, t) = \mathbf{\Psi}_i(x, s, \omega_i)\sin(\omega_i t) \tag{1}$$

The displacement mode shape $\mathbf{\Psi}_i(x, s, \omega_i)$ can be divided into sum of global z-deformation shape of the beam Ψ_{Bi} and total local n-deformation shape of the cross section Ψ_{Ci}:

$$\mathbf{\Psi}_i(x, s, \omega_i) = \mathbf{e}_z \Psi_{Bi}(x) + \mathbf{e}_n \Psi_{Ci}(x, s, \omega_i) \tag{2}$$

This is illustrated in Figure 2.

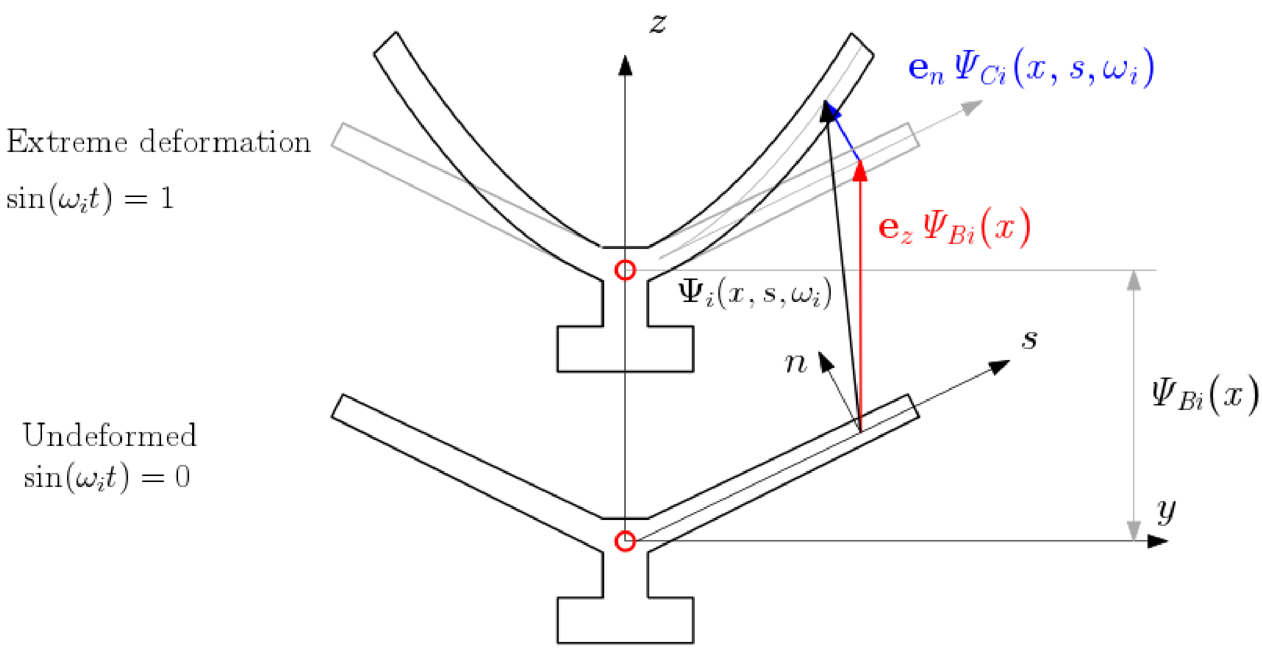

Figure 2.Sketch of the mode shape at location x as sum of global deformation and cross section deformation.

Response of the assumed linear vibration is directly proportional to the excitation amplitude [23]. Due to the long wavelength assumption, the cross section in location x is supported (and excited) only transversally by the global reference point(s). Therefore the local amplitude is directly proportional to the amplitude of the global reference point(s), which equals the global mode shape $\Psi_{Bi}(x)$:

$$\Psi_{Ci}(x,s,\omega_i) = \Psi_{Bi}(x)\Psi_{CR}(s,\omega_i) \tag{3}$$

where Ψ_{CR} is the cross section mode shape relative to the global reference point amplitude i.e. the deformation caused by unit amplitude (z-directional) enforced displacement of global reference point(s). By combining Eq. (2) and Eq. (3), the mode shape gets the form:

$$\mathbf{\Psi}_i(x,s,\omega_i) = \Psi_{Bi}(x)[\mathbf{e}_z + \mathbf{e}_n\Psi_{CR}(s,\omega_i)] \tag{4}$$

2.3 Generalized Mass

Let us consider vibration of mode i as free harmonic vibration of a generalized single degree of freedom system:

$$\xi_i(t) = A_i \sin\omega_i t \tag{5}$$

A is amplitude, and ξ a generalized coordinate, and t time. Kinetic energy of the system can be defined by generalized mass M^* as follows:

$$T_i(t) = \frac{1}{2}M_i^*\dot{\xi}_i^{\,2} = \frac{1}{2}{A_i}^2{\omega_i}^2M_i^*\cos^2\omega_i t \tag{6}$$

The generalized mass can thus be found by considering the peak value of kinetic energy of the vibration mode. That occurs when $\cos^2\omega_i t = 1$. The generalized mass is thus the following:

$$M_i^* = \frac{2T_i^{peak}}{{A_i}^2{\omega_i}^2} \tag{7}$$

The translation kinetic energy of the vibration mode is considered:

$$T_i(\omega_i,t) = \int_0^L \oint \frac{1}{2}\rho(x,s)\theta(x,s)\big(\dot{\mathbf{w}}_i(x,s,\omega_i,t)\big)^2 \mathrm{d}s\mathrm{d}x \tag{8}$$

Velocity is the first time derivative of the deflection shape:

$$\dot{\mathbf{w}}_i(x,s,\omega_i,t) = \omega_i\mathbf{\Psi}_i(x,s,\omega_i)\cos(\omega_i t) \tag{9}$$

The maximum occurs at the moment when the velocity is highest: that occurs when $\cos(\omega_i t) = 1$. The peak kinetic energy of the vibration is thus:

$$T_i^{peak}(\omega_i) = \frac{{\omega_i}^2}{2}\int_0^L \oint \rho(x,s)\theta(x,s)\big(\mathbf{\Psi}_i(x,s,\omega_i)\big)^2 \mathrm{d}s\mathrm{d}x \tag{10}$$

By inserting the mode shape from Eq. (4):

$$T_i^{peak}(\omega_i) = \frac{{\omega_i}^2}{2}\int_0^L \big(\Psi_{Bi}(x)\big)^2 \oint \rho(x,s)\theta(x,s)[\mathbf{e}_z + \mathbf{e}_n\Psi_{CR}(s,\omega_i)]^2 \mathrm{d}s\mathrm{d}x \tag{11}$$

For a prismatic beam with constant mass density distribution in x-direction, this simplifies into:

$$T_i^{peak}(\omega_i) = \frac{{\omega_i}^2}{2}\int_0^L \left(\Psi_{Bi}(x)\right)^2 \mathrm{d}x \oint \rho(s)\theta(s)[\mathbf{e}_z + \mathbf{e}_n \Psi_{CR}(s,\omega_i)]^2 \mathrm{d}s \tag{12}$$

The peak kinetic energy per unit length and unit excitation amplitude can now be defined as *x*-independent term:

$$T_{CR}(\omega) = \frac{\omega^2}{2}\oint \rho(s)\theta(s)(\mathbf{e}_z + \mathbf{e}_n \Psi_{CR}(s,\omega_i))^2 \mathrm{d}s \tag{13}$$

The generalized mass now gets the form:

$$M_i^*(\omega_i) = \frac{2}{{\omega_i}^2 {A_i}^2} T_{CR}(\omega_i)\int_0^L \left(\Psi_{Bi}(x)\right)^2 \mathrm{d}x \tag{14}$$

The integral term can be solved from definition of generalized mass of uncorrected beam solution. That is [23]:

$$M_i = \int_0^L m\left(\Psi_{Bi}(x)\right)^2 \mathrm{d}x \tag{15}$$

$$\Rightarrow \int_0^L \left(\Psi_{Bi}(x)\right)^2 \mathrm{d}x = \frac{M_i}{m} \tag{16}$$

Now the Eq. (14) simplifies into:

$$M_i^*(\omega_i) = \frac{2 M_i T_{CR}(\omega_i)}{m {A_i}^2 {\omega_i}^2} \tag{17}$$

2.4 Generalized Stiffness

Generalized stiffness can be similarly defined by modal strain energy of generalized single degree of freedom system:

$$U_i(t) = \frac{1}{2} K_i^* {\xi_i}^2 = \frac{1}{2} {A_i}^2 K_i^* \sin \omega_i t \tag{18}$$

$$K_i^* = \frac{2}{{A_i}^2} U_i^{peak} = \frac{2}{{A_i}^2}\left(U_{Bi}^{peak} + U_{Ci}^{peak}\right) \tag{19}$$

Strain energy of the global beam deformation U_{Bi} can be written by using generalized stiffness of the uncorrected beam solution. That is:

$$K_i = \frac{2}{{A_i}^2} U_{Bi}^{peak} \tag{20}$$

The strain energy of the cross section deformation U_{Ci} is defined as:

$$U_{Ci}(\omega_i, t) = \frac{1}{2}\int_0^L \oint EI(s)\left[\frac{\partial^2[\Psi_{Ci}(x,s,\omega_i)\sin(\omega_i t)]}{\partial s^2}\right]^2 \mathrm{d}s\,\mathrm{d}x \tag{21}$$

Peak strain energy occurs when the displacement is at its extreme position, i.e. $\sin(\omega t) = 1$. By applying that, and the cross section deformation of Eq. (3) the peak strain energy of the cross section gets the form:

$$U_{Ci}^{peak}(\omega_i) = \frac{1}{2}\int_0^L \oint EI(s)\left[\frac{\partial^2(\Psi_{Bi}(x)\Psi_{CR}(s,\omega_i))}{\partial s^2}\right]^2 \mathrm{d}s\,\mathrm{d}x \tag{22}$$

$$\Rightarrow U_{Ci}^{peak}(\omega_i) = \frac{1}{2}\oint EI(s)\left[\frac{\partial^2 \Psi_{CR}(s,\omega)}{\partial s^2}\right]^2 \mathrm{d}s \int_0^L \left(\Psi_{Bi}(x)\right)^2 \mathrm{d}x \tag{23}$$

In above equation, the *x*-independent term represents peak strain energy per unit length and unit excitation amplitude. It is denoted as:

$$U_{CR}(\omega) = \frac{1}{2}\oint EI(s)\left[\frac{\partial^2 \Psi_{CR}(s,\omega)}{\partial s^2}\right]^2 \mathrm{d}s \tag{24}$$

Now, by applying Eq. (20), Eq. (23) & Eq. (24) into Eq. (19), the corrected modal stiffness can be written as:

$$K_i^*(\omega_i) = K_i + \frac{2}{{A_i}^2} U_{CR}(\omega_i) \int_0^L \left(\Psi_{Bi}(x)\right)^2 \mathrm{d}x \tag{25}$$

By applying Eq. (16) this simplifies into:

$$K_i^*(\omega_i) = K_i + \frac{2M_i U_{CR}(\omega_i)}{{A_i}^2 m} \tag{26}$$

2.5 Frequency by iteration including cross section response analysis

Angular eigenfrequency ω_i of the considered mode *i* can be calculated from generalized stiffness and mass properties as follows:

$$\omega_i = \sqrt{\frac{K_i^*(\omega_i)}{M_i^*(\omega_i)}} \tag{27}$$

However, as can be seen, the generalized mass and stiffness are functions of the angular frequency itself. More specifically, the terms T_{CR} and U_{CR} in Eq. (17) and Eq. (26) are functions of the angular frequency. This relation makes it necessary to use iterative approach to solve Eq. (27).

This is done by separate iteration for each mode *i*. Angular frequency of iteration step *n+1* is obtained from the previous step *n* by following equation:

$$\omega_{n+1} = \sqrt{\frac{K_i^*(\omega_n)}{M_i^*(\omega_n)}} \tag{28}$$

where corrected modal mass and stiffness are obtained from Eq. (17) and Eq. (26).

Initial guess for the frequency is needed for the iteration. In this paper, the initial guess is decided based on the beam solution frequency ω_B and cross section lowest eigenfrequency ω_C. Relation of these frequencies defines the initial guess as presented in Table 1. This definition for initial guess is used in all case studies presented in this paper. However, it is barely a guess that works in cases of this study, but is not general in wider sense.

Table 1. Initial guesses of angular frequency ω_0 based on relation of frequencies of beam solution ω_B and the lowest mode of the cross section ω_C.

Relation of frequencies ω_B & ω_C	**Initial guess ω_0**
$\omega_B \leq 0.9\omega_C$	ω_B
$0.9\omega_C < \omega_B \leq 2\omega_C$	$0.9\omega_C$
$2\omega_C < \omega_B$	$0.99\omega_C$

For n^{th} iteration step, the frequency depended terms in Eq. (17) and Eq. (26) are:

1) $T_{CR}(\omega_n)$. Peak Kinetic energy of unit length of beam cross section under unit enforced z displacement at frequency ω_n.
2) $U_{CR}(\omega_n)$. Peak Strain energy of unit length of beam cross section under unit enforced z displacement at frequency ω_n.

These terms can be calculated by forced vibration analysis of unit length of the cross section in *yz*-plane. Plane strain state is applied in the cross section analysis. Unit displacement in *z*-direction is applied in the global reference point(s) as enforced motion. The energy terms T_{CR} and U_{CR} are solved either once as functions of frequency, or separately for each iteration step. The used option depends on the solution method of the cross section response analysis. The cross section enforced motion analysis can be carried out by any suitable method, analytic or numerical, direct or modal.

The iterative procedure is presented in Figure 3. This iteration will be continued until desired degree of convergence is found. In analyses of this study convergence parameter δ is chosen so that the frequencies of adjacent steps are equal up to 6 significant digits.

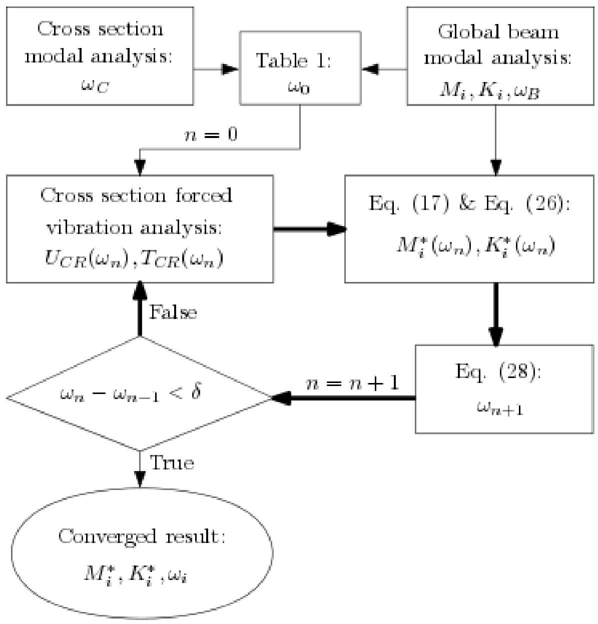

Figure 3.Iterative procedure for the local deformation correction.

2.6 Convergence study and range of validity

Thin-walled cantilever steel beam with symmetric channel section is chosen for convergence study. Beam dimensions are the following: height $h = 0.2$ m, width $b = 0.4$ m, thickness $\theta = 0.007$ m and length $L = 5$ m, and material properties: Young's modulus $E = 206$ GPa, Poisson's ratio $v = 0.3$ and mass density $\rho = 7850$ kgm^{-3}. Geometry of the structure is presented in Figure 4.

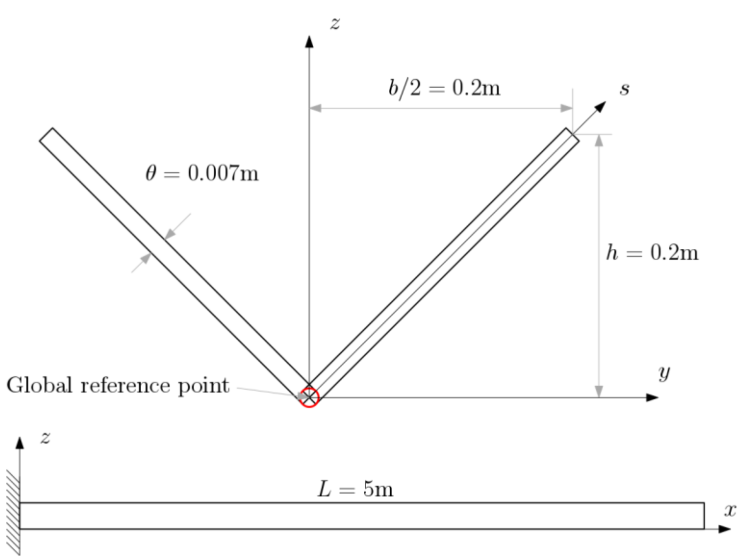

Figure 4. Geometry of the convergence study beam.

First, global modes of the beam are considered. Secondly the cross section behavior is studied under enforced displacement. Then iterative correction of Figure 3 is applied for all modes, and iteration convergence is studied. Finally, the results are compared with fine mesh Finite Element model. The normalized mode shapes are here taken as [24]:

$$B_i \Psi_{Bi}(x) = \sin \beta_i x - \sinh \beta_i x - \left(\frac{\sin \beta_i L + \sinh \beta_i L}{\cos \beta_i L + \cosh \beta_i L}\right)(\cos \beta_i x - \cosh \beta_i x) \quad (29)$$

Numerical values for parameters $\beta_i L$ can be found in [24]. Factors B_i are used to normalize the mode shapes so that maximum absolute deflection is unity. Numerical values of them for the 4 first modes are presented in Table 2. Angular frequencies can be calculated by [24]:

$$\omega_i^2 = \frac{\beta_i^4 EI}{m} \quad (30)$$

Generalized masses can be calculated as follows [23]:

$$M_i = m \int_0^L \Psi_{Bi}(x)^2 dx \quad (31)$$

Generalized stiffness is obtained from the relation between frequency and generalized mass.

$$K_i = M_i \omega_i^2 = \beta_i^4 EI \int_0^L \Psi_{Bi}(x)^2 dx \quad (32)$$

For the studied first 4 modes, the integral term equals with high numerical accuracy the following:

$$\int_0^L \Psi_{Bi}(x)^2 dx \cong 0.25L = \frac{L}{4} \ \forall\ i \in [1,4] \in \mathbb{Z} \quad (33)$$

The resulting numerical values are presented in Table 2. Normalized mode shapes are presented in Figure 5.

Table 2. Parameter values, generalized properties, and frequencies of first 4 flexural modes

Mode number, *i*	**1**	**2**	**3**	**4**
Parameter, $\beta_i L$	1.87510407	4.69409113	7.85475744	10.99554073
Normalization factor, B_i	2.72444111	1.96373507	2.00155221	1.999932886
Generalized mass, M_i	19.42776	19.42776	19.42776	19.42776
Generalized stiffness, K_i	33614	1320155	10350232	39745261
Frequency in Hz, f_i	6.620	41.488	116.167	227.642

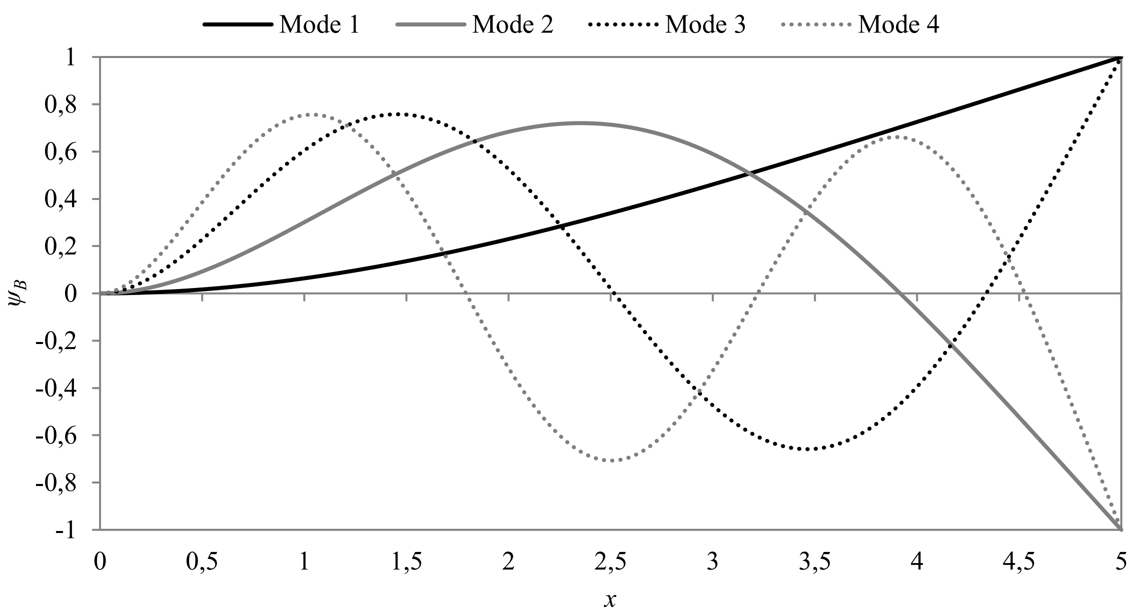

Figure 5. Normalized mode shapes of 4 first modes of the cantilever beam.

Cross section is analyzed under unit amplitude excitation in *z*-direction. The situation is presented in Figure 6. Unit length (in *x*-direction) of cross section is used. Young's modulus is modified to simulate the plane strain state in the cross section plane:

$$E_C = \frac{E}{1-\nu^2} \tag{34}$$

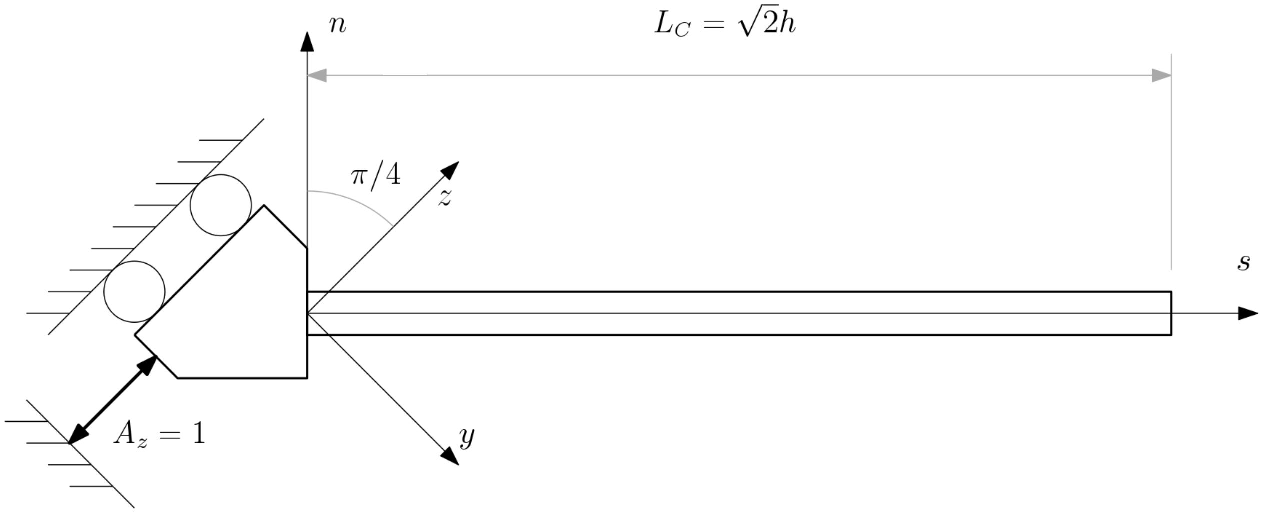

Figure 6. Definition of half cross-section under forced support motion.

At first, the lowest vibration mode of the cross section is defined. The cross section acts as a cantilever beam, similar as Eq. (30):

$$\omega_C{}^2 = \frac{\beta_1{}^4 E_C I_C}{\rho\theta} \tag{35}$$

$$\Rightarrow f_{cs} = 75.9043 \ldots \text{Hz} \tag{36}$$

Forced response to unit motion in z-direction is next considered. This equals the response for $1/\sqrt{2}$ motion in the normal n-direction. Static response r_{sta} to uniform inertia load q is first studied. It follows from Newton's 2nd law:

$$q = \rho\theta a(\omega) = \frac{\rho\theta\omega_i{}^2}{\sqrt{2}} \tag{37}$$

where ω_i is angular frequency of the enforcing motion. Generalized coordinate was defined as response in $s = L_C$ in n-direction. Static response to the uniform inertia load is [25]:

$$r_{sta}(\omega_i) = \frac{qL_C{}^4}{8E_C I_C} = \frac{\rho\theta\omega_i{}^2 L_C{}^4}{8\sqrt{2}E_C I_C} \tag{38}$$

Only the first cross section mode is assumed to have notable effect on the global vibration. Dynamic response of the first mode is found by multiplying the static response by dynamic amplification factor as follows.

$$r_{dyn}(\omega_i) = \frac{r_{sta}(\omega_i)}{1 - \frac{\omega_i{}^2}{\omega_C{}^2}} \tag{39}$$

Now, the shape of relative cross section deformation in n-direction can be written:

$$\Psi_{CR}(s, \omega_i) = \frac{r_{dyn}(\omega_i)}{B_1}\left[\sin\beta_1 s - \sinh\beta_1 s - \left(\frac{\sin\beta_1 L_C + \sinh\beta_1 L_C}{\cos\beta_1 L_C + \cosh\beta_1 L_C}\right)(\cos\beta_1 s - \cosh\beta_1 s)\right] \tag{40}$$

The peak kinetic energy of unit length of the cross section under unit enforced z-motion can now be calculated by Eq. (13):

$$T_{CR}(\omega_i) = \frac{{\omega_i}^2 \rho\theta}{2} \int_0^{L_C} (\mathbf{e}_z + \mathbf{e}_n \Psi_{CR}(s,\omega_i))^2 ds \tag{41}$$

The coordinate transformation of $\mathbf{e}_n$ into y- and z- components yields

$$T_{CR}(\omega_i) = \frac{{\omega_i}^2 \rho\theta}{2} \int_0^{L_C} \left(1 + \frac{\Psi_{CR}(s,\omega_i)}{\sqrt{2}}\right)^2 + \left(\frac{\Psi_{CR}(s,\omega_i)}{\sqrt{2}}\right)^2 ds \tag{42}$$

The symbolical solution of Eq. (42) could be obtained by commercial software, however it is not presented here due to its excessive size. For fluency, numerical solution is presented for parameter values of this case for θ, ρ, L_C, β_1, and B_1:

$$T_{CR}(\omega_i) \approx 0.2828427119 + 0.1565983509 r_{dyn}(\omega_i) + 0.07071067782 r_{dyn}(\omega_i)^2 \tag{43}$$

The peak strain energy of unit length of the cross section under unit enforced z-motion can now be calculated by Eq. (24):

$$U_{CR}(\omega_i) = \frac{E_C I_C}{2} \int_0^{L_C} \left[\frac{\partial^2 \Psi_{CR}(s,\omega_i)}{\partial s^2}\right]^2 ds \approx 68.2931 E_C I_C r_{dyn}(\omega_i)^2 \tag{44}$$

All the information needed for the iterative procedure of Figure 3 is now available. Initial guesses ω_0 are defined based on Eq. (30) & Eq. (35) as shown in Table 1. Global beam properties M_i and K_i calculated by Eq. (31) & Eq. (32) can be found in Table 2. Cross-section forced vibration results U_{CR} and T_{CR} are calculated by Eq. (43) and Eq. (44).

Convergence limit δ is chosen so that the iteration is continued until frequencies of two adjacent iteration steps are same in 6 significant digits. For the first mode, this convergence occurs already after two steps. Second, third and fourth modes require 3, 4, and 4 steps accordingly. The convergence processes are illustrated in Figure 7.

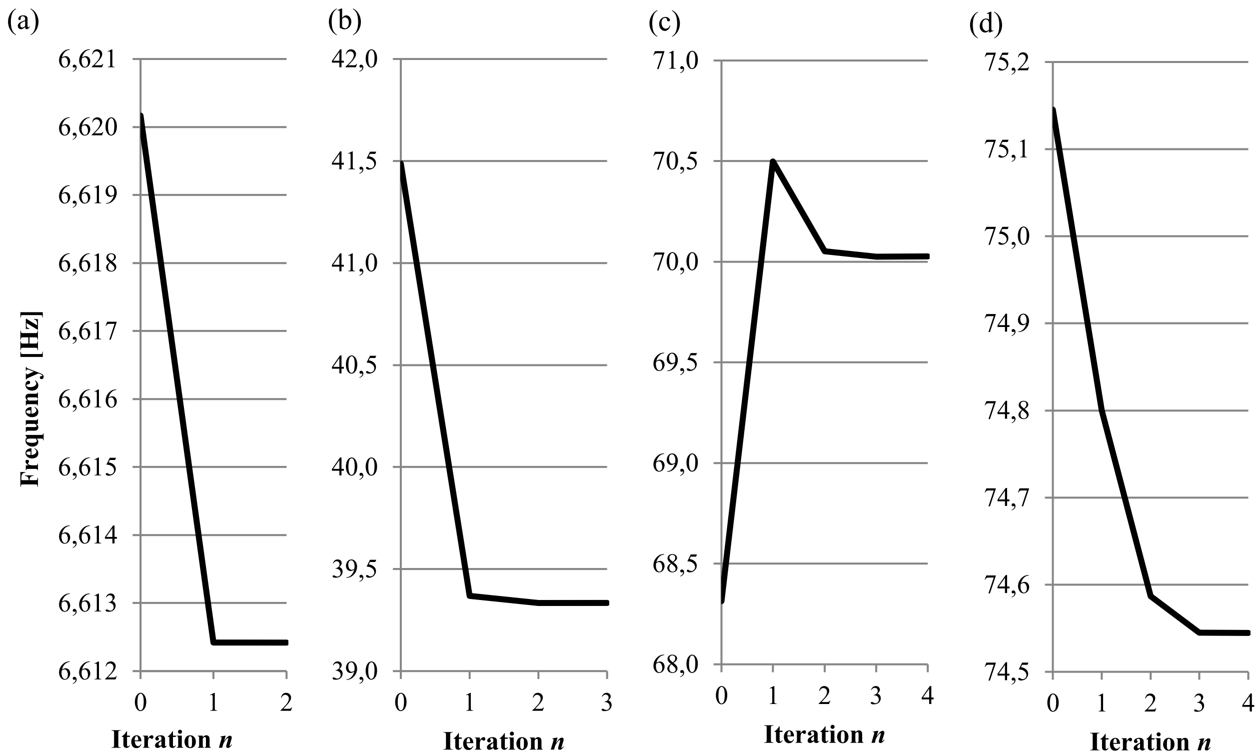

Figure 7. Convergence of the modal frequencies: (a) Mode 1, (b) Mode 2, (c) Mode 3, (d) Mode 4.

Results are validated against Finite Element model consisting of 1600 4 node shell elements. The validation model is solved by NX Nastran 9.0 Finite Element software. Symmetry boundary condition is applied in the symmetry plane. Shell model results are normalized so that global reference line maximum deflection is unity. This makes the generalized mass and stiffness results comparable with the analytical solution. Comparison of results is presented in Table 3.

Table 3. Comparison of results for validation study.

	Mode 1	Mode 2	Mode 3	Mode 4
Generalized Mass [kg]				
Beam	19.428	19.428	19.428	19.428
Corrected Beam	19.518	24.524	276.12	4617.9
Shell FEM	19.560	24.596	185.81	4042.8
Generalized Stiffness [kNm^{-1}]				
Beam	33.614	1320.2	10350	39745
Corrected Beam	33.691	1497.9	53453	1013067
Shell FEM	33.687	1470.1	38093	1042604
Frequency [Hz]				
Beam	6.6202	41.488	116.17	227.64
Corrected Beam	6.6124	39.334	70.026	74.545
Shell FEM	6.6050	38.911	72.062	80.824
Error in Frequency vs. Shell [%]				
Beam	0.23	6.62	61.2	182
Corrected Beam	0.11	1.09	-2.82	-7.77

It can be seen that negative error grows towards higher modes. This is caused by the fact that wavelength is shorter and therefore assumption of infinite wavelength in cross section analysis is no longer valid. This leads to too flexible cross section and thus lowers the combined frequency.

3 Extension to generic case

The theory of Chapter 2 was derived based on the assumptions of Euler–Bernoulli beam theory in both global level and in cross-section analyses. This chapter extends the applicability into more general models as an approximate method.

Extension to generic case is done by assuming that Eq. (17) and Eq. (26) can be used as approximate solutions regardless of the methods used to obtain K, M, T_{CR} and U_{CR}. Validity of this assumption is proven in case studies against fine mesh FEA, and results from literature. The selected case studies represent relevant engineering problems. Effects of separate modelling options in both global and local levels are studied in case study 1, and applicability to periodically stiffened structure in case study 2.

3.1 Implementation into FEM

Applicability of the method into FEM provides great practical importance due to current wide availability of FE-tools. The presented method can be easily used so that K, M, T_{CR} and U_{CR} are solved by FEA. Separate FE-Models are needed for the global level beam and the cross-section analyses. Alternatively, either the global beam, or the cross section can be solved by some other method.

M and K can be obtained by modal analysis of global level beam model. Global beam can be analyzed by any beam model that does not already include inertia induced cross section deformations.

T_{CR} and U_{CR} are obtained by peak kinetic and strain energies of cross section model by enforced support motion analysis. Enforced unit amplitude z-displacement at frequency ω_n is applied in global reference point of the cross section. Cross section can be modeled by in plane beam model or plane strain 2D model. In case of 2D plane strain mesh, special attention should be paid on stiffness of the enforced hard point node. It should be rigidly stiffened into surrounding nodes if there is a risk of significant local movement of the node relative to its adjascents.

3.2 Analysis of periodic structures

In many practical applications of thin walled beams, they are periodically stiffened in transversal direction. Structures that are periodic in x-direction can be analyzed by using 3 dimensional periodic unit FE-model instead of planar model of the cross section. The model can be built up as considered necessary by using different element types including, beam, plate, shell, and 3D solid elements.

Sufficient minimum size for a periodic unit model of example structure is highlighted in Figure 8. Due to symmetry of the stiffeners in the example case, sufficient periodic unit model length L_{PU} is half of the stiffener spacing *S*. Thus only half thickness of the stiffener is included in the periodic unit model.

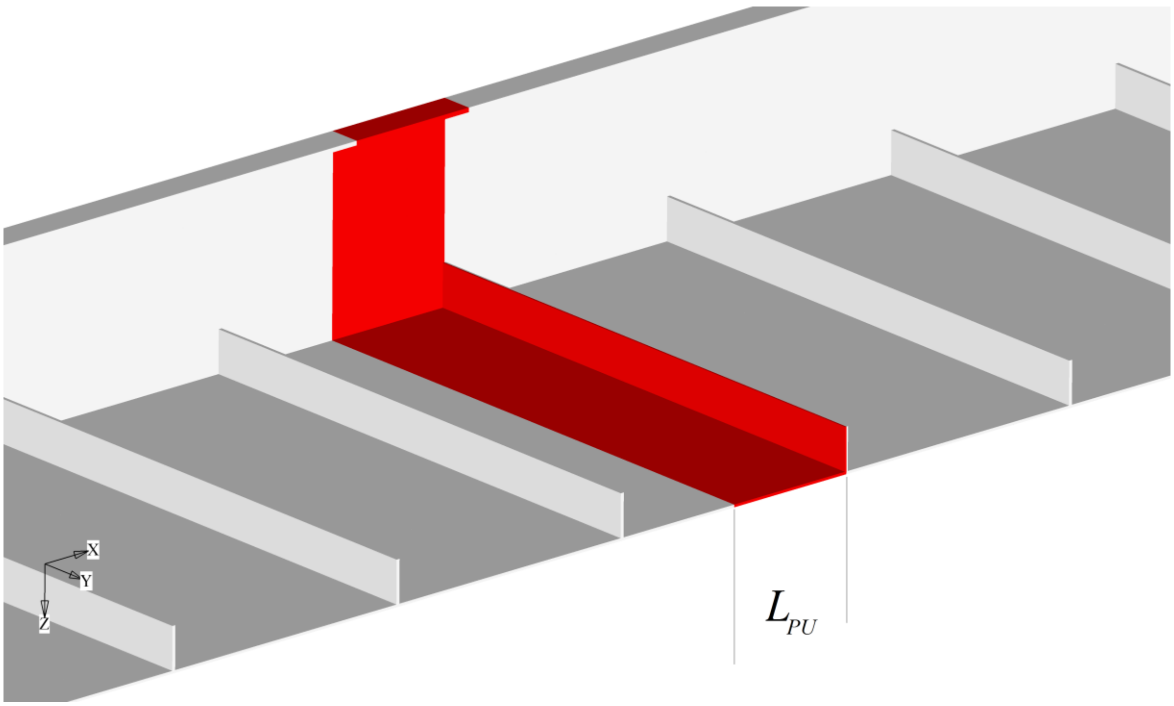

Figure 8. Periodic unit highlighted in a stiffened structure.

The enforced displacement should be applied in the global reference line in whole length of the periodic unit model. Symmetry constraints must be applied in *x*-direction at ends of such model. This approach is reasonable for structures consisting of many similar periodic units i.e. $L_{PU} << L$.

Peak energies obtained by the periodic unit models must be scaled into unit length quantities as follows:

$$T_{CR}(\omega) = \frac{T_{PU}(\omega)}{L_{PU}} \tag{45}$$

$$U_{CR}(\omega) = \frac{U_{PU}(\omega)}{L_{PU}} \tag{46}$$

3.3 Case Study 1: Bridge cross section

Concrete bridge from Refs. [14] & [26] is selected as the first study case. The structure is L_B = 45.72 meters long concrete road bridge with cross section dimensions h = 3.3 m, b = 10.058 m, θ_1 = 0.3 m, θ_2 = 0.4 m. The cross section is presented in Figure 9. The bridge is pinned in both ends. The concrete material is assumed isotropic and linear elastic as in Refs. [14] & [26]. Young's modulus of the concrete is E = 27.793 GPa, Mass density ρ = 2570 kgm^{-3}, and Poisson's ratio υ = 0.2.

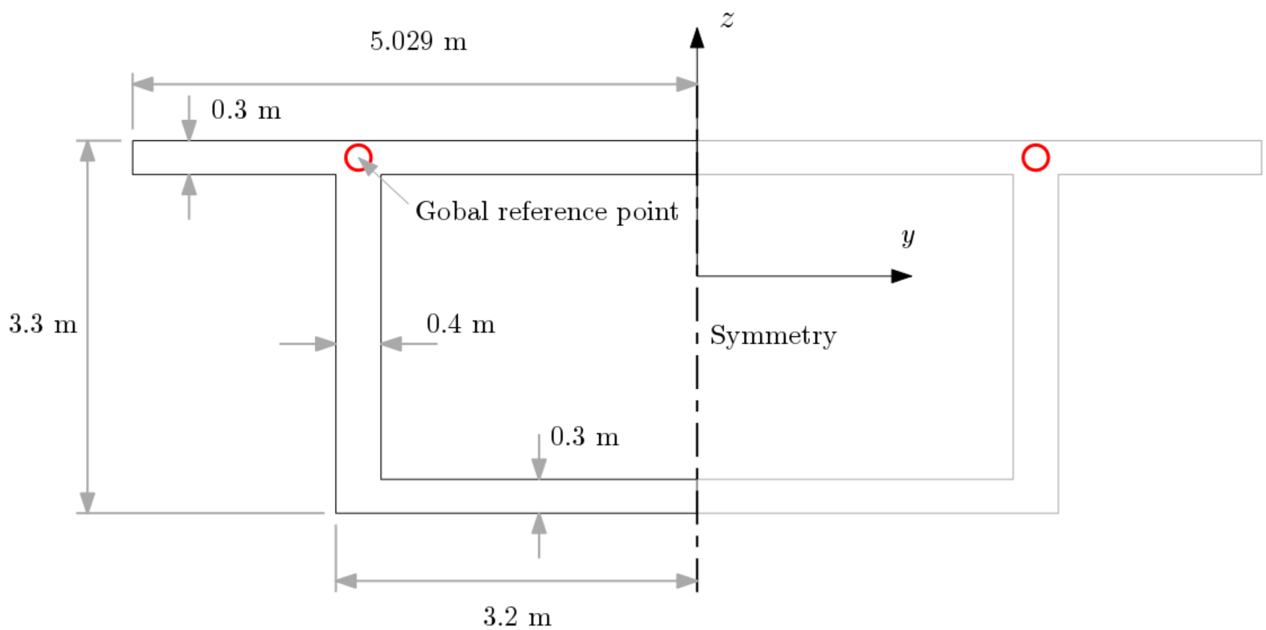

Figure 9.Cross section dimentions of the concrete bridge beam.

The structure is analyzed by several different models to allow comparison of results. Finite element method solver NX Nastran 9.0 is used for all the analyses. Pre- and Post-processing of the models is done with Femap 11.1. software. Global level beam is analyzed by both Euler-Bernoulli and Timoshenko (Nastran PBeam) formulations. Cross section properties of the global beams are obtained by the default cross section tool in Femap 11.1. Cross section deformation is studied by 3 different modelling techniques: Euler-Bernoulli and Timoshenko beams, and 2D plate elements. Additionally, 2 different validation models of the complete structure are created: First by shell elements and second by 3D hexaedral elements. Used models and their size parameters are presented in Table 4.

Table 4. FE-models used in case study 1.

Global beam models	**Elements**	**Nodes**	**DOFs**
Euler Bernoulli	20	21	60
Timoshenko	20	21	60
Cross section models			
Euler Bernoulli beam	29	30	85
Timoshenko Beam	29	30	85
Plane strain plate	533	671	1990
Full models for Validation			
Shell	2902	3032	17579
3D Solid	243126	306862	1836585

Similar mesh is used for both Euler-Bernoulli and Timoshenko beam analyses, only element formulation is changed. The mesh is modeled to run in centerlines of the cross section parts. Furthermore, the validation shell model is created by extruding beam model of the cross section into x-direction. This way mesh sizes and mass distributions in the cross section are similar between the models. Similarly the 3D solid model is created by extruding the plate cross section model. The latter models have 4 elements in plate thickness direction.

All used beam elements are 2 noded, plate and shell elements 4 noded, and solid elements 8 noded. Additionally rigid elements are used in ends of the validation models and as global reference point strengthening in the plate cross section model. Modal solution is used for global beams and validation models, and direct method for cross section analyses. Coupled mass definition is used in all analyses.

Boundary conditions are applied in ends of the global beam. All translations are constrained in $x = 0$, and y- and z- translations in $x = L$. For validation models the constraint is applied in node near the neutral axis that is connected to all cross section nodes by rigid element. Additionally, all nodes in xz-symmetry plane are constrained by y-symmetry (translation in y-direction and rotations around x- and z- constrained). Furthermore in cross section models all nodes are constrained by x-symmetry (translation in x-direction and rotations around y- and z- constrained).

Table 5 presents the modal frequencies by various models, and Table 6 presents the same frequency results as relative error against 3D solid validation model. It can be seen that the influence of local deformation is hardly visible for the first mode. However, the influence increases towards higher modes. In case of the third mode, the local deformation affects the results by similar order of magnitude as the shear deformations and rotational inertia of Timoshenko's beam model. This is caused by the fact that the relative deformation of the cross section increases with the global frequency. This can be seen in Figures 10, 11, and 12. The Figures illustrate the deformation shapes of the analyzed modes by the 3D solid model, and related deformations of the cross section model as part of global Timoshenko beam. The presented cross section deformations are responses for unit amplitude enforced motions acting at the global modal frequencies and applied in the global reference point.

All models with center-line cross sections (Beam models with EB and TB cross sections and the global shell model) are slightly more flexible in comparison to those with actual 2D geometry cross section models (Beam models with shell cross sections and 3D solid model). This is caused mainly because of too long spans between center-line corners, which leads to lower stiffness. Additionally, the T-connection includes double material in the overlapping part, leading to slightly too high mass.

The Timoshenko beam model with shell cross section is kinematic equivalent to the 3D solid model. Thus, comparison of results of these models gives best measure for evaluating performance of the present method. As visible in Table 6, the negative error grows slightly towards the higher modes. This behavior is similar as observed in the convergence study of Chapter 2.6. Thus it seems that the additional assumptions made in the extension to generic case in Chapter 3 do not significantly affect in the performance of the method in this case study.

Figure 10. Mode 1 shape by solid validation model, and cross section response by plate model as part of global Timoshenko beam mode 1.

Figure 11. Mode 2 shape by solid validation model, and cross section response by plate model as part of global Timoshenko beam mode 2.

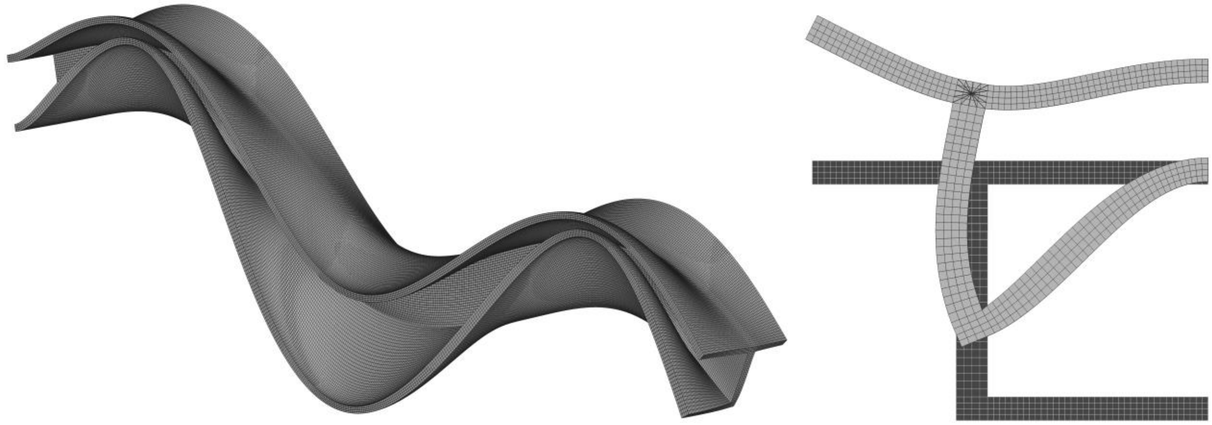

Figure 12. Mode 3 shape by solid validation model, and cross section response by plate model as part of global Timoshenko beam mode 3.

Table 5. Eigenfrequencies of 3 lowest flexural modes of the bridge by different model combinations. EB: Euler-Bernoulli Beam & TB: Timoshenko Beam

Frequency [Hz]	**Mode 1**	**Mode 2**	**Mode 3**
EB model	3.224	12.896	29.016
EB model with EB Cross section	3.214	12.210	21.538
EB model with TB Cross section	3.213	12.188	21.307
EB with Shell Cross section	3.215	12.285	22.361
TB model	3.102	11.222	22.144
TB with EB Cross section	3.093	10.775	18.487
TB with TB Cross section	3.092	10.760	18.386
TB with Shell Cross section	3.094	10.824	18.806
18192 DOF Shell Model	3.080	10.749	18.843
1841172 DOF 3D Solid Model	3.094	10.880	19.390

Table 6. Error in % versus 3D solid validation model by different model combinations.

Error in Frequency vs. 3D solid [%]	**Mode 1**	**Mode 2**	**Mode 3**
EB model	4.21	18.5	49.6
EB model with EB Cross section	3.87	12.2	11.1
EB model with TB Cross section	3.86	12.0	9.88
EB with Shell Cross section	3.91	12.9	15.3
TB model	0.25	3.15	14.2
TB with EB Cross section	-0.04	-0.96	-4.66
TB with TB Cross section	-0.05	-1.09	-5.18
TB with Shell Cross section	-0.01	-0.51	-3.01
18192 DOF Shell Model	-0.45	-1.20	-2.82

Table 7 Presents the iteration steps needed for convergence. All calculated model combinations find convergence within 5 steps. Table 8 presents comparison with literature results with similar definitions. The presented results are in agreement with those of [26] and [14].

Table 7. Iteration steps required for 6 significant digit convergence in frequency.

Iterations until convergence	**Mode 1**	**Mode 2**	**Mode 3**
EB model with EB Cross section	2	3	5
EB model with TB Cross section	2	3	5
EB with Shell Cross section	2	3	4
TB with EB Cross section	2	3	3
TB with TB Cross section	2	3	3
TB with Shell Cross section	2	3	3

Table 8.Comparison with literature. [26] Euler Bernoulli beam & [14] Euler Bernoulli beam with cross section deformations.

Frequency [Hz]	**Mode 1**	**Mode 2**
EB model	3.2239	12.896
EB model with EB Cross section	3.2137	12.210
Huang et al. [26]	3.2200	12.962
Hamed&Frostig [14]	3.1720	12.067

3.4 Case study 2: Ship transversal deck beam

The second case study provides example of a periodic structure. The considered structure is a transversal (here x-directional) deck beam typical for passenger ships. Typical ship deck is continuous, and includes similar beams with constant spacing, here b = 2.5 m. Model of the considered beam is presented in Figure 13. Symmetry in y-direction is applied in both sides of the beam to model continuity of the deck. The beam consists of a T-profile connected to a deck plate that is stiffened by perpendicular (y-directional) flat bar stiffeners. The beam is supported in z-direction by 4 supports between the clamped ends (x-deformation is unconstrained in $x=L$). Spans between the supports are: 3.6 m, 5.4 m, 6 m, 5.4 m, and 3.6 m in that order.

The T-beam consists of 0.45 m high web of 0.007 m thickness and 0.15 m wide flange of 0.01 m thickness. The deck plate is 0.006 m thick and has 0.1 m high and 0.008 m thick flat bar stiffeners with spacing 0.6 m. Additionally, the deck plate has evenly distributed non-structural mass 40 kgm^{-2} on it. Material properties are: Young's modulus E = 206 GPa, Poisson's ratio v = 0.3 and mass density ρ = 7850 kgm^{-3}.

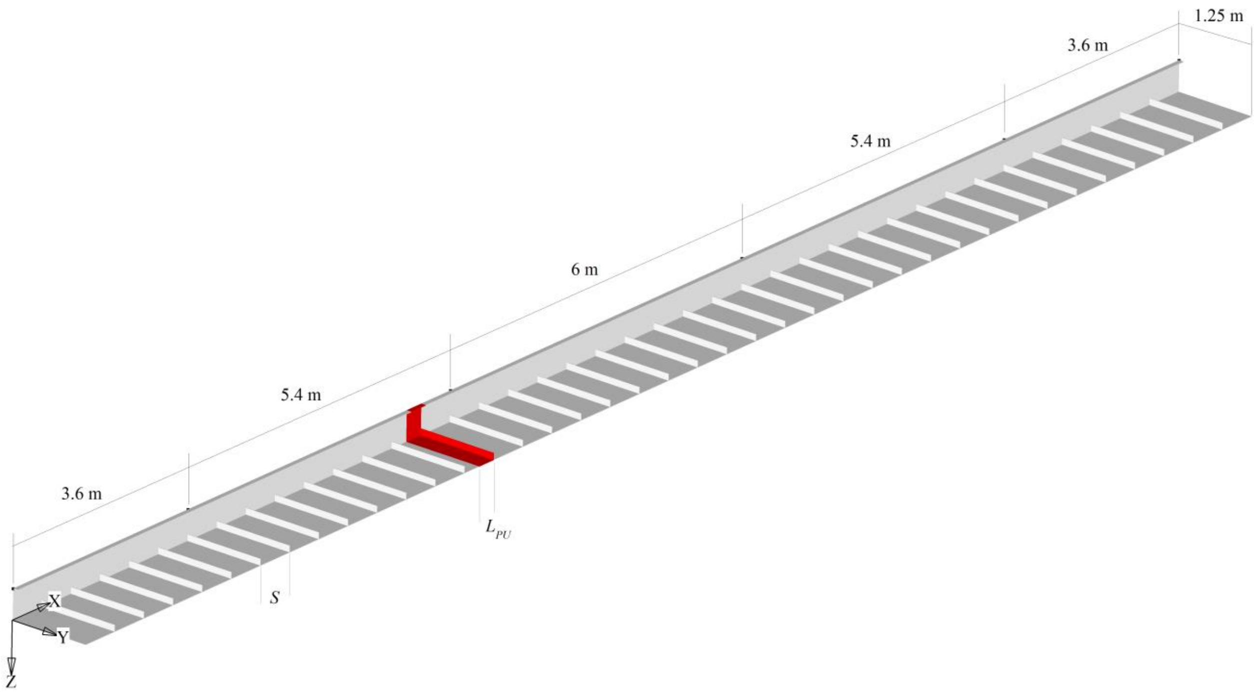

Figure 13. Dimensions of the (half) deck beam structure.

FE model consisting of 40 2-noded Nastran PBeam (Timoshenko beam) elements is used for the global modal analysis. Periodic unit model is needed for finding U_{PU} & T_{PU} for equations (45) & (46). The 0.3 meter long model consists of 63 4-noded shell elements. The results are validated against shell element model with similar mesh size as the periodic unit model. Mesh sizes of the shell element models are about 0.1 meters per element. Properties of the FE-models of this case study are presented in Table 9

Table 9. FE-models used in case study 2.

	Elements	**Nodes**	**DOFs**
Global beam model	40	41	114
Periodic unit model	63	84	294

Validation shell model	4549	4806	22742

Two sets of global beam bending stiffness properties are applied. In the first case properties are taken directly from the Femap 11.1. cross section tool. In the second case, they are calculated separately to include axial stiffening effect by transversal stiffeners [27] and the effective breadth of the deck plate flange [28].

Young's modulus for the deck plate part of the cross section is given in [27]:

$$E_{deck} = \frac{E}{1-\upsilon^2\left(1+\frac{A_S}{S}\right)} = 231.461\ldots\,\text{GPa} \tag{47}$$

Above, A_S is cross section area of a stiffener, and S is spacing of the stiffeners. The effective breadth of the deck plate is taken from [28]:

$$b_e = \frac{4\lambda\sinh^2(\pi b/\lambda)}{\pi(1+\nu)[(3-\nu)\sinh(2\pi b/\lambda)-2(1+\nu)(\pi b/\lambda)]} \tag{48}$$

In Eq. (48), b is total breadth of the beam (2.5 m), and λ deformation wavelength of the considered deformation shape. Average wavelength for the beam length is used. The wavelength is based on the assumption that number of waves in internally supported beam with clamped ends is 1 plus a half wave for each internal support for the first mode, and half wave more for each higher mode. Average wavelengths, effective breadths, and effective second moments of area for the first 3 modes are presented in Table 10.

Table 10. Assumed average wavelengths, effective breadths, and effective (half cross section) second moments of area for the first 3 modes.

	# of waves	λ	b_e	$I^*/2$
Mode 1	3	8 m	1.4998... m	1.9335… × 10^{-4} m^4
Mode 2	7/2	48/7 m	1.3107... m	1.8722…× 10^{-4} m^4
Mode 3	4	6 m	1.1535... m	1.8116…× 10^{-4} m^4

Mode shapes of the first 3 modes by global beam model are presented in Figure 14. Figure 15 presents periodic unit responses at corresponding modal frequencies. Figures 16, 17 and 18 present modes 1, 2, and 3 of the validation model respectively.

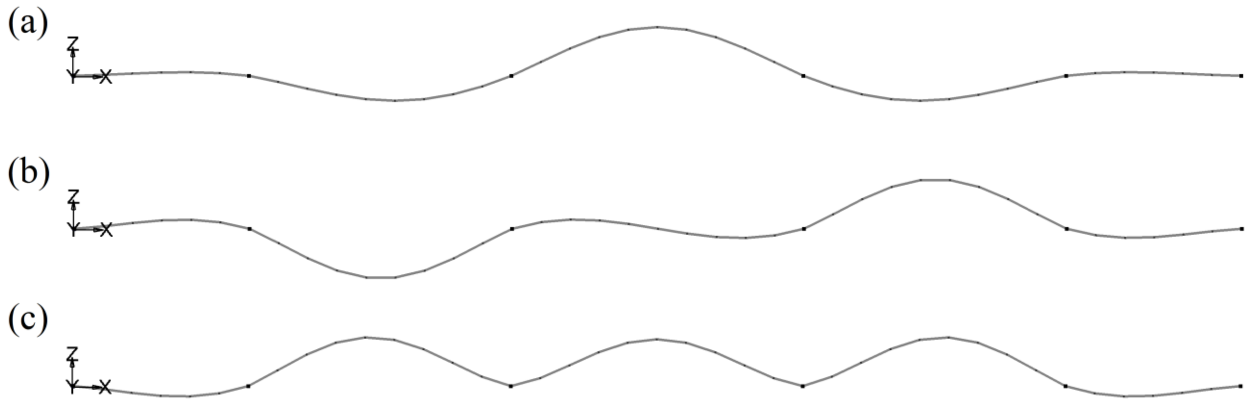

Figure 14. Mode shapes by global beam model: (a) Mode1, (b) mode 2, and (c) Mode 3

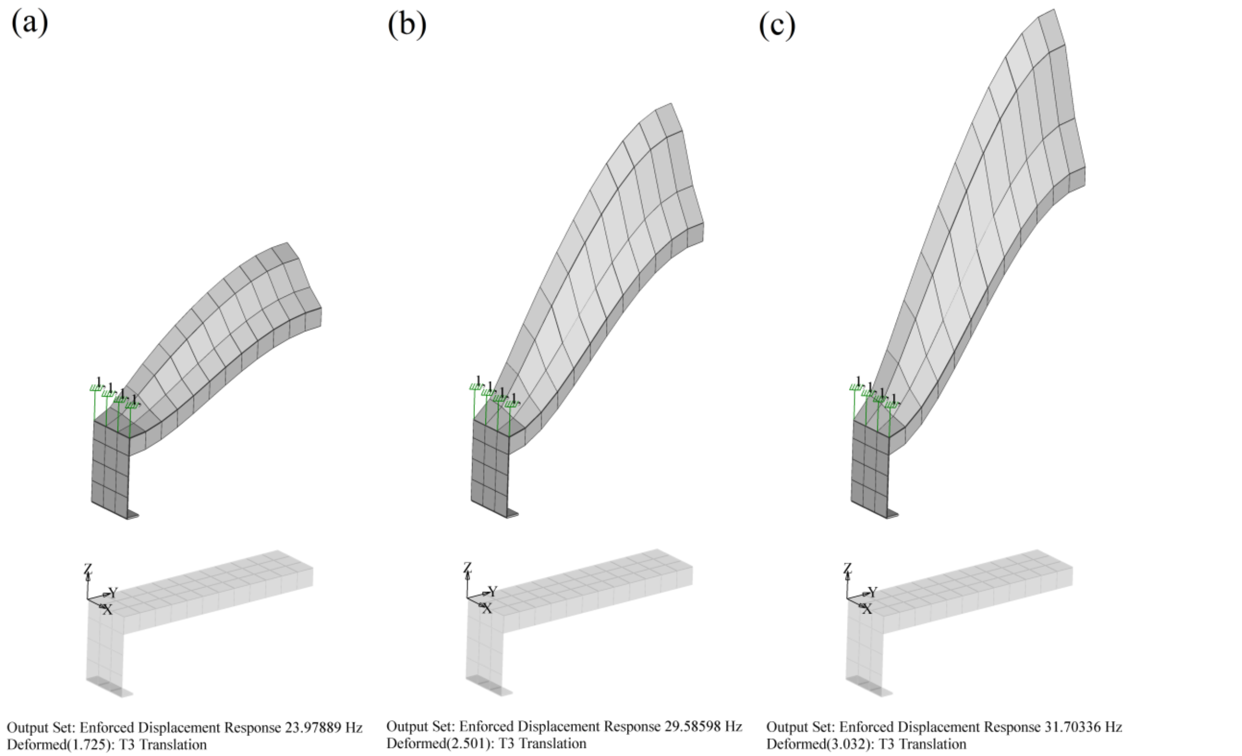

Figure 15. Responses of periodic unit model excited by unit amplitude forced excitation of final frequency of: (a) global mode 1, (b) global mode 2, and (c) global mode 3.

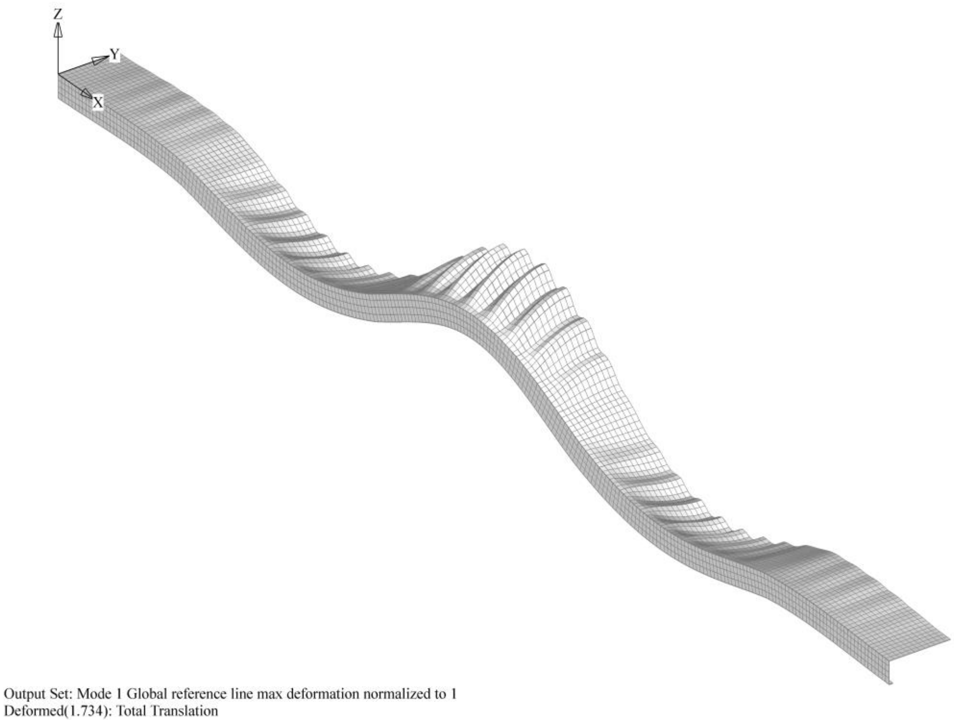

Figure 16. Mode 1 of the validation shell FE-model.

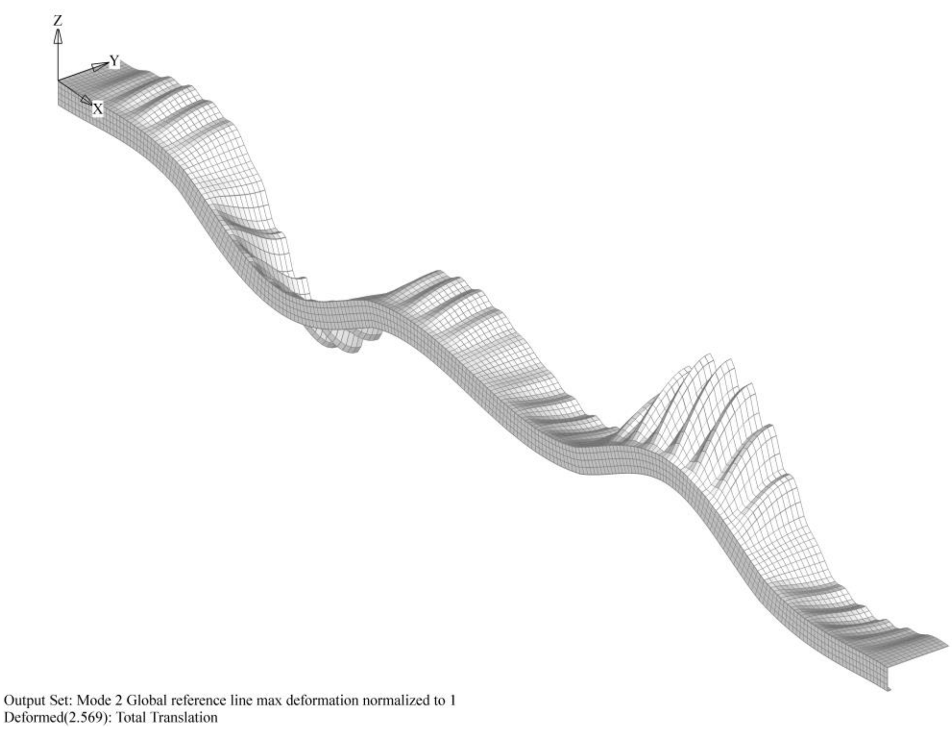

Figure 17. Mode 2 of the validation shell FE-model.

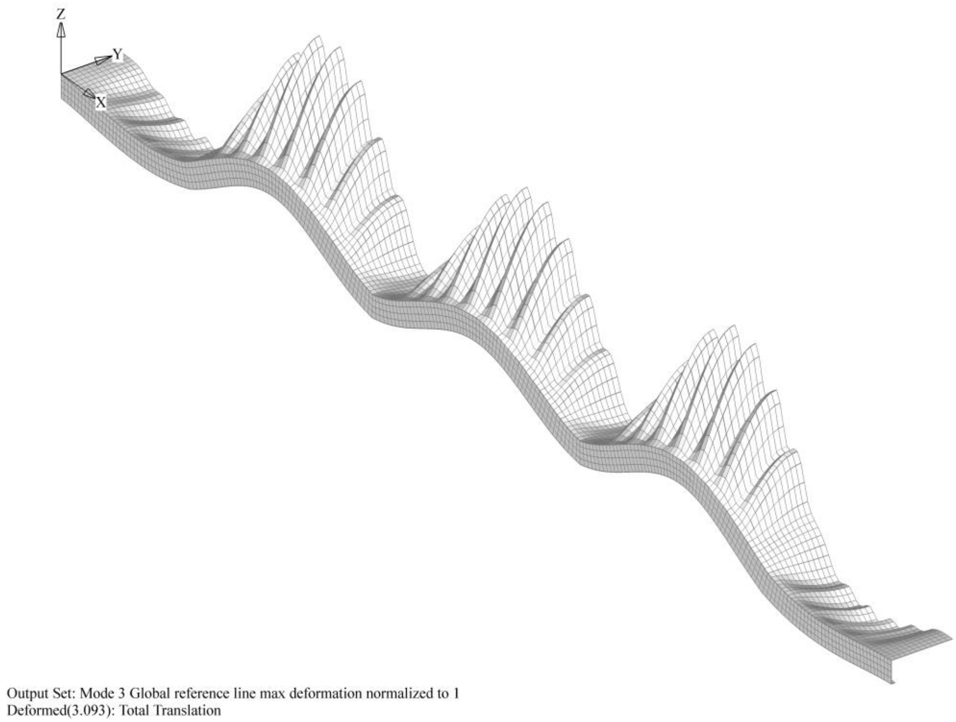

Figure 18. Mode 3 of the validation shell FE-model.

Comparison of modal masses, stiffnesses and frequencies are presented in Table 11. The results by the present methods match with the validation model results with excellent accuracy, especially when effective breadth and deck plate stiffness are used for the beam anaylsis.

Table 11. Results comparison of case study 2.

	Mode 1	**Mode 2**	**Mode 3**
Generalized mass [kg]			
PBeam FEMAP 11.1. default	6.00×10^2	7.66×10^2	1.03×10^3
PBeam with b_{ef} [28] and E_{deck} [27]	6.00×10^2	7.66×10^2	1.02×10^3
Present method with default PBeam	1.05×10^3	2.21×10^3	4.00×10^3
Present method with b_{ef} [28] and E_{deck} [27]	1.04×10^3	2.11×10^3	3.71×10^3
Shell model	1.06×10^3	2.12×10^3	3.81×10^3
Generalized stiffness [Nm^{-1}]			
PBeam FEMAP 11.1. default	1.81×10^7	4.42×10^7	7.80×10^7
PBeam with b_{ef} [28] and E_{deck} [27]	1.77×10^7	4.23×10^7	7.31×10^7
Present method with default PBeam	2.43×10^7	7.84×10^7	1.64×10^8
Present method with b_{ef} [28] and E_{deck} [27]	2.36×10^7	7.31×10^7	1.47×10^8
Shell model	2.41×10^7	7.24×10^7	1.50×10^8
Frequency [Hz]			
PBeam FEMAP 11.1. default	27.63	38.25	43.91
PBeam with b_{ef} [28] and E_{deck} [27]	27.30	37.39	42.52
Present method with default PBeam	24.19	29.97	32.20
Present method with b_{ef} [28] and E_{deck} [27]	23.98	29.59	31.70
Shell model	23.98	29.42	31.53
Error of frequency vs. Shell [%]			

PBeam FEMAP 11.1. default	15.2	30.0	39.3
PBeam with b_{ef} [28] and E_{deck} [27]	13.8	27.1	34.8
Present method with default PBeam	0.88	1.87	2.13
Present method with b_{ef} [28] and E_{deck} [27]	-0.02	0.55	0.54
Iterations for 6 digit convergence			
Present method with default PBeam	4	6	6
Present method with b_{ef} [28] and E_{deck} [27]	4	6	6

4 Conclusion

This study presented a correction of beam modal properties by modifying its modal stiffness and mass according to kinetic and strain energies involved in cross section deformation. The correction itself is independent of solution methods used for the subproblems: Modal analysis of the beam global level, and enforced support motion response analysis of the cross section. Therefore, it is possible to apply the correction with any structural models and analytical or numerical solving methods, or any combination of them. This makes it possible to use detailed numerical models where necessary, while carrying out straightforward parts of the problem effectively by simple analytical formulae. This kind of approach has value in conceptual design of structures in which the accuracy of solutions must be reasonable, while the computational cost must be extremely light.

The method requires iterative solution of the frequency, involving cross section response analysis in each step. It was shown in on open channel cross-section that the convergence of iteration is very fast and accurate results can be found with only 2-4 iterations. The frequency results are in good agreement with 3D-Finite Element analysis used for validation. However, the method tends to slightly underestimate the frequencies towards higher modes. This is caused by assumption of infinite wavelength in cross section analysis.

The method was tested for relevant case studies. Case study on closed bridge cross-section from Ref. [14] showed that the present method allows shear deformations and rotational inertia to be taken into account in both global beam level analysis and cross section analysis. This leads to improved accuracy in flexural modes. The second case study considered a T-beam attached to a stiffened panel, which is typical structure in passenger ship decks. The study showed that the presented method is suitable for analysis of periodically stiffened beams. The agreement between the proposed method and the 3D-FEA was found to be very good in all case studies.

The study was limited to beam bending problems with respect to their symmetry plane. Transverse bending or torsional modes that are important for example in the bridge applications are not included in this paper. Extending the applicability of the presented method for the torsional modes is left for further work. Further studies are needed for studying applicability of the method for analyses involving damping.

5 Acknowledgments

This work was supported by: Intercity Collaboration of South-West Coast of Finland (LOURA); and Meyer Turku OY. The financial support is gratefully acknowledged by the authors.

6 References

[1] L. Euler, De curvis elasticis, Bousquet, Lausanne and Geneva, 1744.

[2] S. P. Timoshenko, On the corrections for shear of the differential equation for transverse vibrations of prismatic bars, Philosophical Magazine 41 (1921) 744–746.

[3] S. P. Timoshenko, On the transverse vibrations of bars of uniform cross section, Philosophical Magazine 43 (1922) 125–131.

[4] I. Senjanović & N. Vladimir, Physical insight into Timoshenko beam theory and its modification with extension, Structural Engineering and Mechanics, 48 (2013) 519-545.

[5] T. Kaneko, On Timoshenko's correction for shear in vibrating beams, Journal of Physics D, 8 (1975) 1927–1936.

[6] J. R. Hutchinson, Shear coefficients for Timoshenko beam theory, Journal of Applied Mechanics, 68 (2001) 87–92.

[7] J. Jensen, On The Shear Coefficient In Timoshenko's Beam Theory, Journal of Sound and Vibration, 87 (1983) 121-135.

[8] I. Senjanović, and Y. Fan, The bending and shear coefficients of thin-walled girders, Thin-Walled Structures, 10 (1990) 31-57.

[9] F. C. Smith, and D. M. Howard, Calculation and Measurement of Normal Modes of Vibration of an Aluminum-alloy Box Beam with and Without Large Discontinuities, NACA-TN-2884, 1953.

[10] B. Budiansky, and R.W. Fralich, Effects of panel flexibility on natural vibration frequencies of box beams, NACA-TN-3070, 1954.

[11] R. G. Thomson, and E. T. Kruszewski, Cross sectional deformations of monocoque beams and their effects on the natural vibration frequencies, NASA TN-D-987, 1961.

[12] S. Ali Hasan, Linear vibration of thin-walled beams of equal angle-section, Journal of sound and vibration 32 (1974) 3–23.

[13] M. J. Klausbruckner, and R. J. Pryputniewicz, Theoretical and experimental study of coupled vibrations on channel beams, Journal of Sound and Vibration 183 (1995) 239-252.

[14] E. Hamed, and Y. Frostig, Free vibrations of multi-girder and multi-cell box bridges with transverse deformations effects, Journal of Sound and Vibration 279 (2005) 699–722.

[15] E. Carrera, G. Giunta, and M. Petrolo, Beam Structures: Classical and Advanced Theories, John Wiley & Sons, Ltd., Chichester, 2011.

[16] R. Bebiano, N. Silvestre, and D. Camotim, Local and global vibration of thin-walled members subjected to compression and non-uniform bending, Journal of Sound and Vibration 315 (2008) 509–535.

[17] E. Carrera, G. Giunta, P. Nali, and M. Petrolo, Refined beam elements with arbitrary cross section geometries, Computers and Structures 88 (2010) 283–293.

[18] E. Carrera, M. Petrolo, and P. Nali, Unified formulation applied to free vibrations finite element analysis of beams with arbitrary section, Shock and Vibration 18 (2011) 485–502.

[19] M. Petrolo, E. Zappino, and E. Carrera, Refined free vibration analysis of one-dimensional structures with compact and bridge-like cross sections, Thin-Walled Structures 56 (2012) 49–61

[20] E. Carrera, E. Zappino, and M. Filippi, Free Vibration Analysis of Thin-Walled Cylinders Reinforced With Longitudinal and Transversal Stiffeners, Journal of Vibration and Acoustics 135 (2013).

[21] E. Carrera, A. Pagani, and F. Zangallo, Thin-walled beams subjected to load factors and non-structural masses, International Journal of Mechanical Sciences 81 (2014) 109–119.

[22] A. Pagani, F. Zangallo, and E. Carrera, Influence of Non-Structural Localized Inertia on Free Vibration Response of Thin-Walled Structures by Variable Kinematic Beam Formulations, Shock and Vibration (2014)

[23] R.W.Clough, and J. Penzien, Dynamics of Structures, Second Edition, McGraw-Hill Inc, New York, 1993.

[24] R. D. Blevins, Formulas for Natural Frequency and Mode Shape, Krieger Publishing Company, Malabar, Florida, 1979, Re-issued 1995.

[25] J. M. Gere, and S. P. Timoshenko, Mechanics of Materials, Third edition, PWS-KENT, Boston, 1990.

[26] D. Huang, T. Wang, and M. Shahawy, Vibration of thin-walled box-girder bridges excited by vehicles, American Society of Civil Engineers Journal of Structural Engineering 121 (1995) 1330–1336.

[27] A. Laakso, J. Romanoff, H. Remes, and A. Niemelä, An analytical metod for cabin deck fundamental frequency, in: C. Guedes Soares, and J. Romanoff (Eds.), Proceedings of the 4th international conference on marine structures (MARSTRUCT 2013), Espoo, Finland, 25-27 March 2013, CRC Press/Balkema, Leiden, 2013, pp. 53-60.

[28] J. K. Paik, Some recent advances in the concepts of plate-effectiveness evaluation, Thin-Walled Structures, 46 (2008) 1035-1046.